Energy Conversion and Management: X 26 (2025) 101001

Contents lists available at ScienceDirect

Energy Conversion and Management: X

journal homepage: www.sciencedirect.com/journal/energy-conversion-and-management-x

A state-of-the-art micro-mixing micro-combustor with enhanced flame stabilization characteristics using H_2-air mixtures

Sreejith Sudarsanan [a], Akram Mohammad [b], Prabhu Selvaraj [a], Khalid A. Juhany [b], Radi A. Alsulami [c], Sudarshan Kumar [d], Ratna Kishore Velamati [a,*]

[a] Department of Mechanical Engineering, Amrita School of Engineering, Coimbatore, Amrita Vishwa Vidyapeetham, India
[b] Department of Aerospace Engineering, Faculty of Engineering, King Abdulaziz University, Jeddah, Saudi Arabia
[c] Department of Mechanical Engineering, Faculty of Engineering, King Abdulaziz University, Jeddah, Saudi Arabia
[d] Department of Aerospace Engineering, Indian Institute of Technology Bombay Powai, Mumbai 400076, India

ARTICLE INFO

Keywords:
Micro-combustion
Stability limit
Hydrogen
Micro-mixing
Partially premixed
Lift-off

ABSTRACT

A novel micro-mixing micro-combustor was developed and the flame stabilization characteristics were investigated numerically. The Combustor exhibited excellent lean stability limits, with stability limits increasing as the fuel–air mixture became leaner. Stability limits achieved for the equivalence ratios 1.0, 0.8 and 0.6 were 8 m/s, 14 m/s and 16 m/s respectively (although the exact blow-off limit for each case is expected to be higher). The limits are higher than those reported in previous studies on hydrogen fueled combustors. As the Reynolds number exceeded 500, simulations above 6 m/s were performed using a turbulent model to account for the transition to turbulence. An all-new criterion to predict the flame stabilization was suggested by specifying the range of local equivalence ratio at central slot interface (φ_{inter}) as $7 \leq \varphi_{inter} \leq 21$ (cold flow) for both laminar and turbulent regimes when $0.6 \leq \varphi_g \leq 1.0$. The uniformity of wall temperature demonstrated significant improvement at lean equivalence ratios in both the laminar and turbulent regimes, which is crucial for practical applications such as thermoelectric generators (TEGs) and similar systems. Furthermore, the introduction of micro-mixing resulted in the transformation of the diffusion flame into a partially premixed flame. The underlying mechanisms driving this transformation in flame structure were analyzed and discussed in detail. Regarding the enhancement of stability limits, the firing rates of existing combustors were compared with the that of the present combustor and the results revealed a significant 28 % hike at the lift-off condition, which would be even higher when the exact blow-off limits are determined.

1. Introduction

The requirement of reliable and long-lasting miniaturized power generators has been the need of this era, which subsequently leads to the replacement of chemical batteries with micro-combustors that work with fuels such as hydrocarbons [1], ammonia [2–5], hydrogen [6–8] etc. However, there are several challenges to be overcome in the process of designing such a combustion based micro-device. The major factors which affect the stable performance of a micro-combustor includes the type of fuel, type of combustion, combustor geometry, wall material, nature of application etc. Although these fuels possess substantially higher energy density compared to conventional batteries, hydrogen is widely recognized as the most prominent candidate for not only its zero emission properties but also for its high energy density and large stability range owing to its high laminar burning velocity. While the availability of fuel is an advantage on the implementation of hydrogen as fuel, the storage and transportation of hydrogen poses as a hurdle. Nevertheless, even this hindrance is overcome to a great instant by the introduction of innovative technologies [9].

However, results obtained from various researches with different fuels are compared in this section. Raghavan et al [10] numerically analyzed the effect of position of a deflector along with a centrally slotted bluff body in a quartz micro-combustor with hydrogen as fuel. The study revealed that the average combustion efficiency and exhaust gas temperature were considerably improved. In addition, the flame tip opening phenomenon was mitigated. The best performance was achieved when the deflector was placed midway of the combustor. Cai et al [11] experimentally investigated the dynamics of premixed flames for ultra-lean mixtures using CH_4 as fuel. For higher Reynolds numbers (Re)

* Corresponding author.
E-mail addresses: v_ratnakishore@cb.amrita.edu, ratnavk@gmail.com (R.K. Velamati).

https://doi.org/10.1016/j.ecmx.2025.101001
Received 8 January 2025; Received in revised form 22 March 2025; Accepted 1 April 2025
Available online 3 April 2025

Nomenclature

MEMS	Micro-electro mechanical systems
Phi	Equivalence ratio
TPV	Thermo-photo voltaic
TEG	Thermo-electric generator
PPF	Partially Premixed Flame
W_0	Combustor wall thickness, mm
H_1	Bluff body central slot thickness, mm
H_0	Combustor height, mm
H_2	Air inlet port height, mm
L_0	Combustor length, mm
L_1	Bluff body length, mm
W_1	Bluff body thickness, mm
W_2	Bluff body tip thickness, mm
L_3	Width of micro-mixing slot, mm
K_n	Knudsen number
Re	Reynolds number
$\boldsymbol{\rho}$	Density of fluid, kg/m^3
η_c	Combustion efficiency, %
$\vec{\boldsymbol{u}}$	Velocity component, m/s
P	Gas pressure, Pa
k_f	Thermal conductivity of the fluid, W/m-K
h_j	Enthalpy of jth species, J/kg
h	Natural heat transfer coefficient, W/mˆ2-K
T_w	Outer wall temperature, K
T_∞	Ambient temperature, K
φ_g	Global equivalence ratio
V_{air}	Inlet air velocity, m/s
$\boldsymbol{\Phi}_{inter}$	Equivalence ratio at the central slot interface
Z	Mixture fraction
Z_{stoic}	Stoichiometric mixture fraction
HRR	Heat Release Rate, W/m^3
NPF	Non-Premixed Flame
PPF	Partially-Premixed Flame
MM	micro-mixing

and higher equivalence ratios (Φ = 0.8 and 1.0), the wall temperature was also found to be higher. Combustion efficiency, however, was lower at a low equivalence ratio (Φ = 0.6). Devi et al. [12] numerically studied the effect of vortex generator location on combustion efficiency in a H_2-air planar combustor. They observed that the highest combustion temperature and heat of reaction occurred when the vortex generator was placed near the inlet. George et al [13,14] deduced that the bluffer the body becomes, the periodic vortex shredding increases and more mixing occurs. Sankar et al. [15] provided a comprehensive review on the implementation of liquid fuels in micro- and *meso*-scale combustion. Tang et al [16] conducted a comparative study experimentally on combustion characteristics of methane, propane and hydrogen in a micro-planar combustor and observed a wider flame stability range for hydrogen-air mixture. Moreover, the minimum flammable channel height for each fuel was observed to be 1 mm, 2 mm and 2.5 mm for hydrogen, propane and methane respectively. So, ultimately in terms of several variables regarding fuel type, hydrogen qualifies as the best choice over other fuels for its high laminar burning velocity, zero emission, availability and low quenching distance.

Considering the next parameter combustor design, several geometrical modifications are adopted to extend the stability limits. The various modifications to the combustor geometry include bluff bodies [17], cavities [18], deflectors [10], catalytic surfaces [19], porous media [20,21], trapezoidal ribs [22], nozzles [23], double-channel counter-flow configurations [24], and Swiss-roll designs [25] etc. Among which centrally slotted bluff body demonstrates better stabilization by facilitating the formation of diffusion flames. As He et al [26] reported, the blow-off limit of hydrogen was enhanced to 792 cm^3/s by using a centrally slotted bluff body. Raghavan et al [27] was able to stabilize hydrogen-air flames to a firing rate of 420 cm^3/s and analyzed the effect of central slot width. Li et al [28] reported a blow-off limit of 34 m/s for hydrogen using a centrally slotted bluff body for a blockage ratio of 0.55. Another important parameter is the selection of wall material. The aspects to be considered include the capacity to withstand high temperature, good thermal conductivity, ease of fabrication and excellent corrosion resistance. Since stainless steel satisfies all these requirements [29–31] it is chosen as the combustor wall material.

Apart from factors such as type of fuel, geometric modifications and wall material, another key parameter or rather the most important is the nature of combustion. combustion is classified as premixed [11,32,33], diffusion [25,34,35] and partially-premixed combustion [1,36–38]. Wan et al [39] experimentally and numerically investigated the combustion characteristics of H_2-air micro-combustor with a bluff body and the results showed that the blow off limit is extended significantly by the introduction of bluff body at lower equivalence ratios. Wan et al [40] also proposed a double layer micro-disc-combustor with annular step and Swiss-roll structure and conducted experimental investigation on flame dynamics. The results revealed that as Re decreases, blow-off limit increases first and then decreases. Additionally, the average temperature and heat transfer of upper wall decrease linearly with the decrease in Re. However premixed combustion has limitations, such as flashback and low stability limits [41], which can be prevailed over by diffusion combustion, where fuel and oxidizer are supplied separately into the micro-combustor and get mixed and then burned. Nevertheless, proper mixing is essential for diffusion combustion, which can be achieved by using a combustor that is sufficiently long or geometrically modified (enhanced mixing). Micro mixing is a method that enables partially premixed combustion rather than diffusion combustion in large scale combustion, since a small amount of oxidizer is allowed to get mixed with fuel before their actual mixing occurs. The micro-mixing combustor prototype exhibits superior combustion performance at the rated fuel temperature of 473 K, as demonstrated by the research [42] in the revised manuscript. This includes an outlet temperature distribution factor of 6.56 %, a combustion efficiency of 99.99 %, and a NO emission of 4.70 μL/L at 15 % O_2. According to the research source [43], micro-mixing provides exceptional stability, enabling the reduction of the oxygen-fuel (OF) ratio to 21 % (by volume) without the need for hydrogen (H_2) enrichment. It is clear that MM combustion with H_2 enrichment is a suggested technique for gas turbines that require variable fuel/oxidizer combustion with controlled emissions. The three-dimensional cold flow field of a unique Micro-mix model burner, which is based on numerous confluent parallel round jets, was studied experimentally and numerically by Liu et al. [44]. Between D = 3d, 4167 ≤ Red ≤ 20,878, the flow field at the Micro-mix burner's exit is independent of the Reynolds number. The potential energy core affects the velocity in the area where the jets converge, and jet deformation occurs beyond this convergence zone. The RANS results can be matched with the experimental results in a good trend.

The literature analyzed, motivated to incorporate micro-mixing in micro-combustor and investigate the flame stabilization characteristics of hydrogen. To the authors' knowledge, having the methodology of micro-mixing is not yet implemented in micro scale combustors, the research becomes a novel one. Additionally considering the transformation of flame structure from diffusion to partially premixed is not only expected to change the flame structure but also to improve the stability limits. Moreover, as suggested by the literature, numerous

studies have been conducted to increase the stability limits by modifying geometry as well as introducing fuel blends. This study attempts to develop a novel micro-mixing combustor design that incorporates micro-mixing to enhance the stability limits of hydrogen combustion, which also eliminates the possibility of flashback. To realize this, numerical investigation is conducted to analyze the flame dynamics and stability of hydrogen. The combustion system investigated features a centrally slotted bluff body micro-combustor, combined with a micro-mixing slot, designed to improve mixing and flame stability.

2. Numerical methodology

1.1. Combustor model

While determining the combustor dimensions, most of these literatures used a combustor height of 1 or 1.1 mm, but the authors were eager to investigate the flame stabilization of slightly higher dimensions, so that the combustor can be conveniently and precisely fabricated. So, the combustor height was chosen as 4 mm and all the other dimensions were chosen in such a way that accurate fabrication is possible. The schematic model of the combustor with a centrally slotted bluff body incorporating a micro-mixing slot is illustrated in Fig. 1 (i). The total length (L_0) of the combustor is taken as 80 mm with a height (H_0) of 4 mm. Hydrogen is supplied through the central slot of bluff body of height (H_1) 1 mm, whereas air is supplied through the upper and lower ports of the same height. The length (L_1) of the bluff body is 10 mm. The thickness of bluff body and the combustor walls (H_2) is 0.5 mm. A micro-mixing slot with a width of 0.6 mm (L_3) is incorporated in the bluff body at a distance (L_2) of 5.4 mm away from the tip. The micro-mixing slot angle (θ_0) is set to 45^0.

2.2. Mathematical model

Flow is considered continuous as the Knudsen number (Kn) was found to be significantly lower than the crucial value of 0.01 (Kn = 32.5×10^{-6} for the present work). Laminar flow was considered when the maximum Reynolds number (Re) was below 500, while a turbulent model was used for values when Re > 500 [45–47]. As reported by Wang et al. [48], Li et al. [28] and others, a two-dimensional model should be used instead of a three-dimensional model when the aspect ratio exceeds nine, as the difference in results become negligible. In the present study, the combustor width (50 mm) is significantly greater than its height (4 mm). Therefore, a 2-D model was chosen for the current investigation in order to reduce the computing effort without compromising the accuracy of the results.

Governing equations are as given below:

Continuity equation:

$$\nabla.(\rho\,\vec{u}) = 0 \tag{1}$$

Momentum equation:

$$\rho(\vec{u}.\nabla\vec{u}) = -\nabla P + \nabla.(\mu\left[\nabla\vec{u} + (\nabla\vec{u})^{T} - \frac{2}{3}\nabla.\vec{u}I\right]) \tag{2}$$

Energy equation in fluid:

$$\nabla.\vec{u}\,(\rho E_t + P) = \nabla.\left[k_f\nabla T - \left(\sum_j h_j\vec{J_j}\right)\right] + S_f \tag{3}$$

Energy equation in solid:

$$\nabla.(\vec{u}\rho h) = \nabla.[k_s\nabla T] \tag{4}$$

Species transport equation:

$$\nabla.\left(\rho\vec{u}Y_j\right) = \nabla.\vec{J_j} + \omega_j \tag{5}$$

Diffusion flux, $J_j = -\sum_{j=1}^{N-1}\rho D_{i,j}\nabla Y_j - \rho D_{T,j}\frac{\nabla T}{T}$ where $-\rho D_{i,j}\nabla Y_j$ = Molecular diffusion

$-\rho D_{T,j}\frac{\nabla T}{T}$ = Thermal diffusion

ρ is the density of the fluid, $\vec{u}$ is the velocity component, k_f and k_s are the thermal conductivity of the fluid and solid, P is the gas pressure, E_t is the fluid energy and S_f is the source term. h_j and $\vec{J_j}$ are enthalpy and diffusion flux of j^{th} species. $D_{T,j}$ and D_{ij} are the thermal diffusion coefficient and multi component mass diffusion coefficient for the species 'i into j' calculated from Maxwell-Stefan equations [49].

2.3. Numerical framework

Selection of material for the combustor and bluff body walls is the first variable in present numerical setup, for which stainless steel was chosen for its several properties such as high strength, corrosion resistance, ability to withstand high temperatures, ease of fabrication etc. Next the reaction mechanism by Keromnes et al [50] (10 species and 29 reactions) was adopted in the present numerical methodology as it was well refined and tested for low, moderate and extreme conditions like

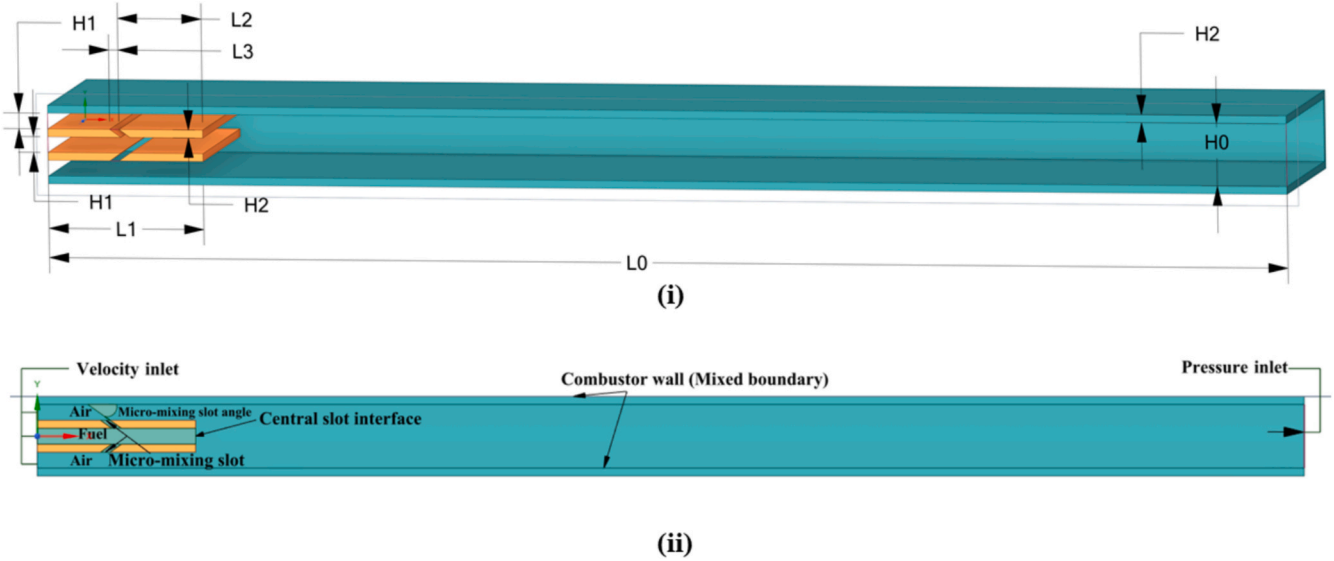

Fig. 1. (i) 3-D Sectional view of the micro-combustor model (ii) Combustor boundary conditions.

high pressure (1 – 70 bar) and high temperature (900 – 2500 K). Furthermore, the boundary conditions are specified as displayed in Table 1.

Heat transfer from outer wall to surroundings was calculated by Eq.:

$$q'' = h(T_w - T_\infty) + \varepsilon_w \sigma((T_w)^4 - (T_\infty)^4) \quad (6)$$

where h denotes the natural convection heat transfer coefficient (20 W/(m^2.K)) [17]; T_w, T_∞ represent outer wall and ambient temperatures respectively. ε_w represents the emissivity of material (0.6) [51] and σ is the Stephan-Boltzman constant (5.67 x 10^{-8} W/ (m^2.K^4)).

The software FLUENT 2023R1 was used to conduct numerical simulations. The second order upwind approach was used to discretize the continuity, momentum, energy, and species equations, and the "SIMPLE" algorithm was employed to handle the pressure–velocity coupling. The ideal gas law was used to compute the density of the gaseous mixture. Stiff chemical solver was used to increase iteration convergence. When the residuals of all governing equations were less than or equal to 10^{-6}, numerical simulations were deemed to have converged. To start the combustion, a temperature field of 2400 K was set up downstream of the bluff body where a combustible mixture is expected to be present. As the Reynold's number was calculated to be less than 500 (Re = 496.26 at V_{air} = 6 m/s), laminar model was considered and when it crossed 500 (Re = 744.38 at V_{air} = 8 m/s), turbulent model was considered [45]. To accommodate the turbulent flow characteristics, realizable K-ε model [52,53] was adopted.

2.4. Mesh independence and validation

To analyze the computational efficiency and accuracy, the geometric model was divided into structured grid systems with three different cell sizes (a) Δx = Δy = 0.025 mm, (b) Δx = Δy = 0.0125 mm and (c) Δx = Δy = 0.00625 mm. Simulations were performed for V_{air} = 2 m/s and stoichiometric global equivalence ratio for these three grid systems and the results were compared as shown in Fig. 2. The temperature along the axial centerline of the combustor is considered to represent the flame temperature, while the mole fraction of OH species defines the flame zone. As the results exhibit similar characteristic, the grid system (a) Δx = Δy = 0.025 mm was selected to reduce computational efforts without compromising the accuracy.

The experimental validation of the present model is impossible due to the novelty of the model. Moreover, experimental researches on combustor with slotted bluff body is not reported yet. Hence the authors have chosen the experimental investigation of a combustor with bluff body and performed numerical simulations with the present methodology and then compared the experimental and numerical results. Finally, the authors were able to find the results are in close agreement and the methodology was validated. Wan et al [39] conducted experiments and numerical (two-dimensional turbulent) investigation to determine the blow-off limit of hydrogen flames in a micro-combustor with bluff body for lean mixtures (equivalence ratios from 0.4 to 0.6). The same analysis was repeated numerically using the current methodology and the results are compared in Fig. 3. The results exhibit a close agreement and resulted in a maximum error of 9.5 % compares with experimental results as well as 4.8 % with the numerical results.

Table 1
Boundary conditions.

Boundary Conditions		
Name	Type	Specification
Fuel inlet	Velocity inlet	Temperature – 300 K
Air inlet	Velocity inlet	Temperature – 300 K
Outlet	Pressure outlet	Pressure – 1 atm
Combustor wall	Mixed boundary	Convection and Conduction No slip

The close concurrence of the present results with the experimental and numerical ones validates the current numerical set up and methodology given the nature of the problem.

Additionally, the authors performed computations for the experimental configurations given by Meyer et al. [54] (from TNF workshop). The configuration is hydrogen-air non premixed jet flames (75 % H_2 + 25 % N_2) in an air co-flow nozzle. The numerical radial variation of temperature and O_2 mole fraction at different axial locations (x/D = 5 and 20) using the present methodology are compared with experimental results in Fig. 4. The results are in close agreement and the maximum error is found to be 10 %. Moreover, the trend of the plots at each scenario matches well each other and hence the present numerical model is able to predict diffusion flames reasonably well.

3. Results and discussion

Numerical simulations were performed for stoichiometric and lean equivalence ratios starting at an inlet velocity (air) of 2 m/s and then it is incremented at an interval of 2 m/s to study the flame stabilization characteristics. Up to an inlet velocity of 6 m/s, the maximum Reynolds number remained below 500, and therefore, a laminar flow model was applied. However, at higher inlet velocities, due to the transformation of flow behavior, turbulent model was adopted. In the first section, the flame stabilization characteristics in the combustor in the laminar regime have been discussed.

2.1. Laminar flame stabilization characteristics

2.1.1. Local and global mixing performance

The local mixing performance was analyzed by measuring and comparing the local equivalence ratio at the central slot interface (marked in Fig. 1 (ii)). The central slot interface plays a crucial role in the micro-mixing phenomenon, as the flame stability completely depends on the equivalence ratio at that location. To establish a criterion for flame stabilization, numerical simulations were performed and converged for non-reacting flow (cold condition) over an inlet air velocity range of 2 to 6 m/s and various equivalence ratios. Then the equivalence ratio at the central slot interface (ϕ_{local}) was measured and plotted in Fig. 5 (i). The developed criterion for stable flames in the laminar regime is that stable combustion occurs when the local equivalence ratio at the interface (cold flow) lies within the range $7 < \phi_{local} < 21$, for global equivalence ratios of 1.0, 0.8, and 0.6.

Initially cold flow for all velocities (2–16 m/s) at each equivalence ratio (0.6–1) was preformed and the value of local equivalence ratio at central slot interface (φ_{local}) was measured for each case and tabulated. Then hot flow (combustion) was conducted for each case and checked for flame stabilization. It was observed that for the cases where the value of φ_{local} exceeds 21(cold flow), the flame was blown off the combustor (hot flow). The lowest value for φ_{local} obtained in the present study is '7'. Subsequently the correlation between cold flow and hot flow was formulated and $7 \leq \varphi_{local} \leq 21$ was determined as the flame stabilization criterion. The advantage of the criterion is that from cold flow itself, i.e., merely by running the cold flow and measuring φ_{local}, the flame stability limits can be predicted. However, investigation of leaner mixtures may lead to lower values of φ_{local}, which requires further analysis to determine the stabilization regime.

The global mixing performance was investigated by introducing a mixing coefficient (ξ) which is calculated using the equation:

$$\xi = 1 - \frac{X_{H_2,\ \text{lower wall}}}{X_{H_2,\ \text{Centre axis}}} \quad (7)$$

Non-reacting (Cold) simulations were performed at different inlet velocities (keeping ϕ_g = 1.0 and 0.6) and the results are demonstrated in Fig. 5 (ii). The condition where value of 'ξ' is 0.2 is considered as the criterion of sufficient mixing occurrence and the corresponding axial

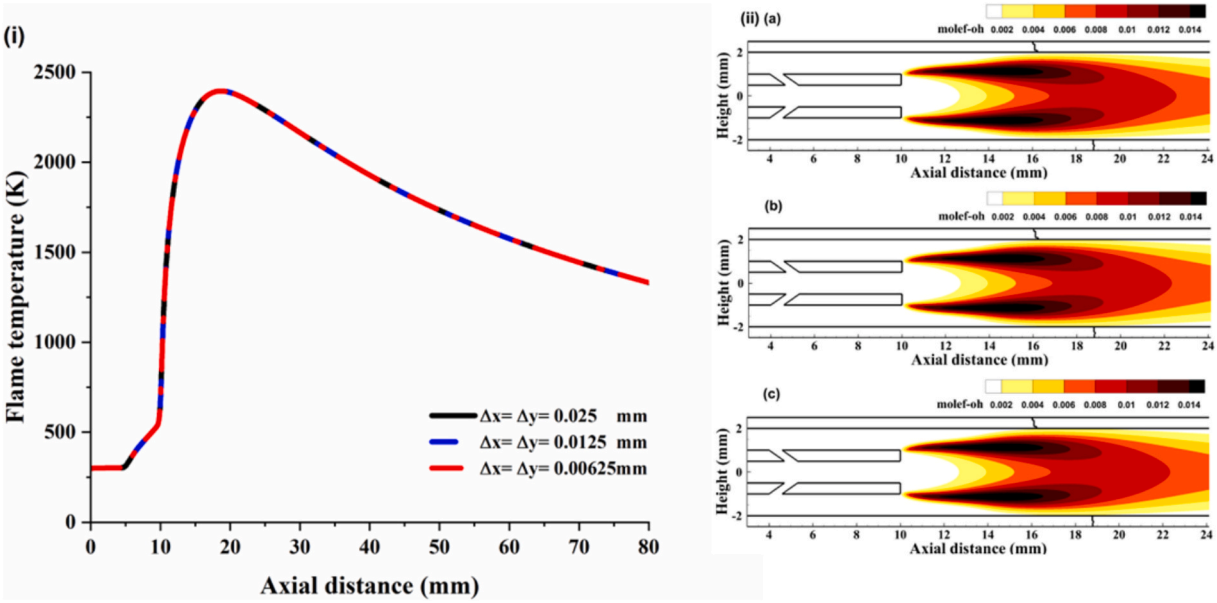

Fig. 2. Comparison of (i) Flame temperature and (ii) OH mole fraction of three grid systems: (a) Grid1 – $\Delta x = \Delta y = 0.025$ mm (b) Grid2 – $\Delta x = \Delta y = 0.0125$ mm (c) Grid3 – $\Delta x = \Delta y = 0.00625$ mm at $V_{air} = 2$ m/s and stoichiometric global equivalence ratio

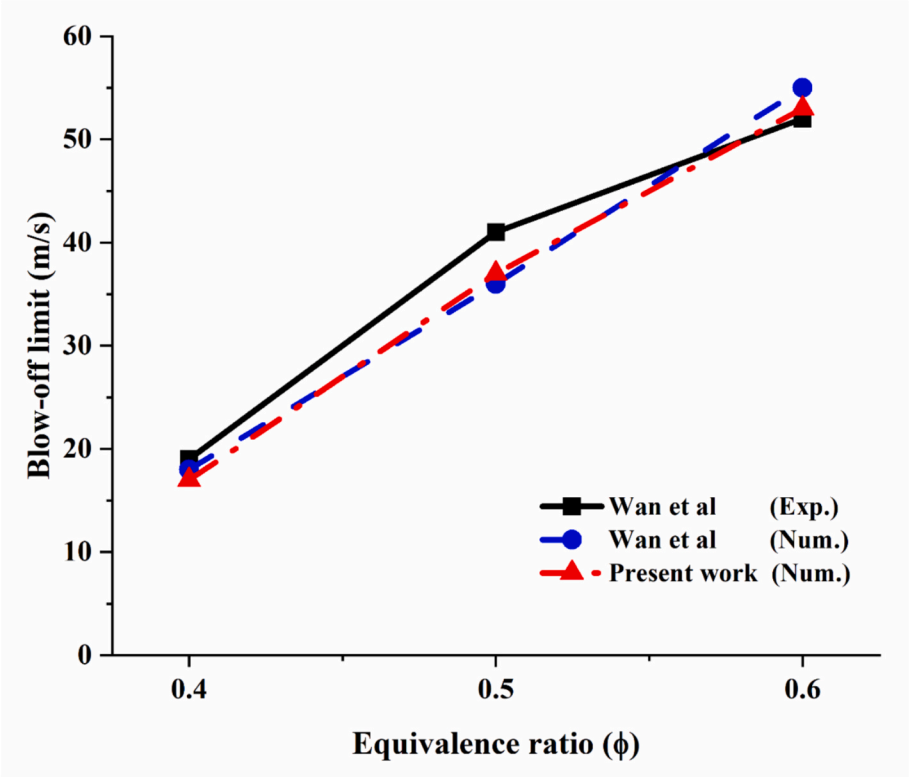

Fig. 3. Flame blow-off limit at lean equivalence ratios from 0.4 to 0.6 (a) Wan et al (Exp.)[39], (b) Wan et al (Num.)[39] and (c) Present work (Num.).

location is the mixing location [55]. As expected, the most efficient global mixing performance was observed at the lowest velocity ($V_{air} = 2$ m/s, $\phi_g = 1.0$) having$\xi = 0.2$ at the axial location of 26.6 mm from the combustor inlet. Mixing performance deteriorated with an increase in inlet velocity, as the axial location of sufficient mixing moved downstream and it reached 59 mm when the velocity was 6 m/s. To understand the enhancement in mixing performance, 'ξ' for $\phi_g = 0.6$ at the same velocities were also plotted in Fig. 4 (ii), which demonstrates a similar trend, but better compared to that of $\phi_g = 1.0$. This is due to the lower fuel content in the mixture, which enhances the mixing performance. The flame stabilization characteristics for the reacting flow is being discussed in the next section.

2.1.2. *Effect of inlet velocity and global equivalence ratio*

The variation in flame structure and location with inlet velocity is depicted in Fig. 6 (i) and (ii). Flame structure is represented by the heat release rate (HRR), which was calculated by dividing heat of reaction by cell volume (W/m^3). For stoichiometric global equivalence ratio, a

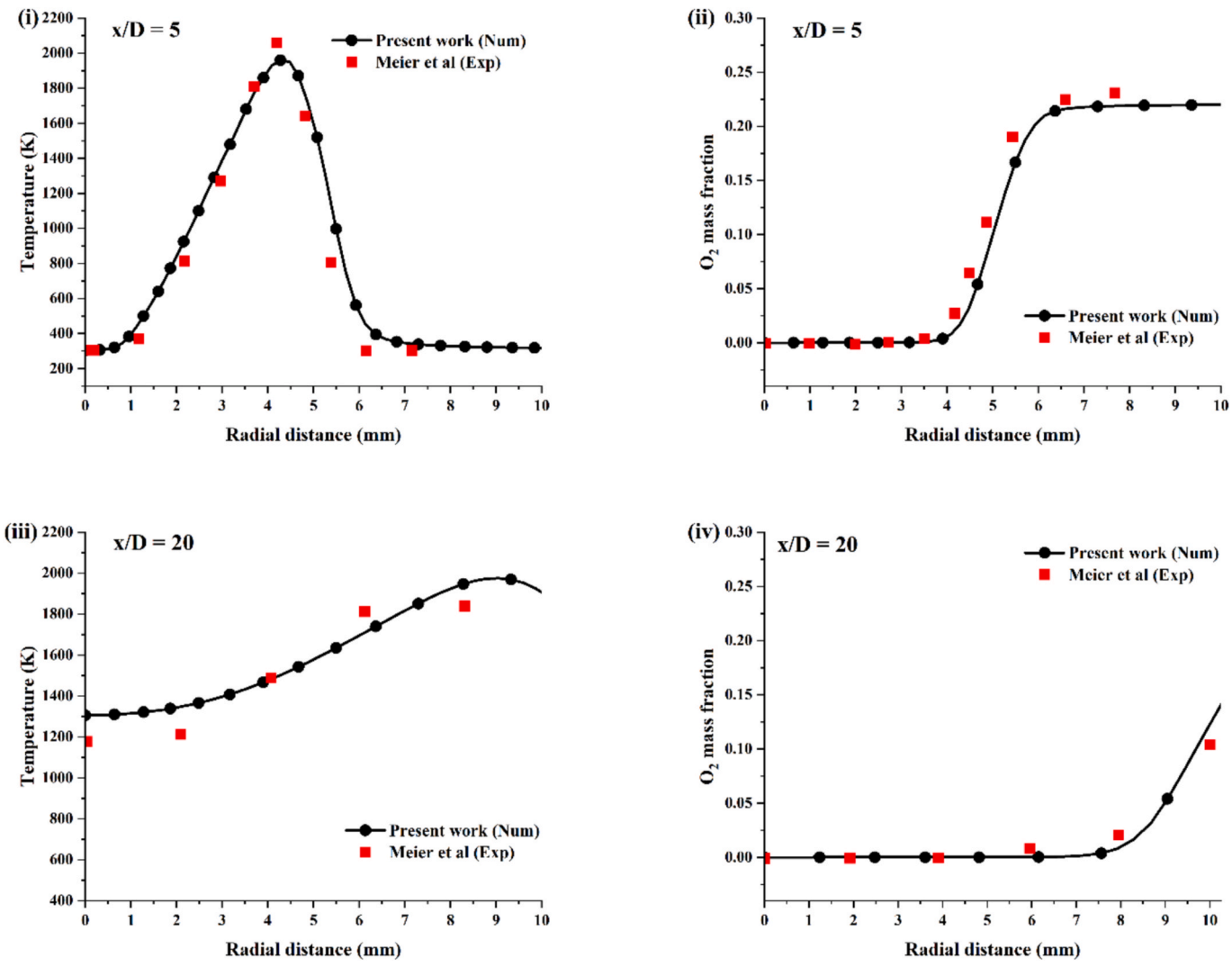

Fig. 4. Comparison of present numerical and experimental results (Meyer et al [54]) (i) Radial distribution of temperature (ii) Radial variation of O_2 mass fraction at an axial location of x/D = 5 and (iii) Radial distribution of temperature (ii) Radial variation of O_2 mass fraction at an axial location of x/D = 20.

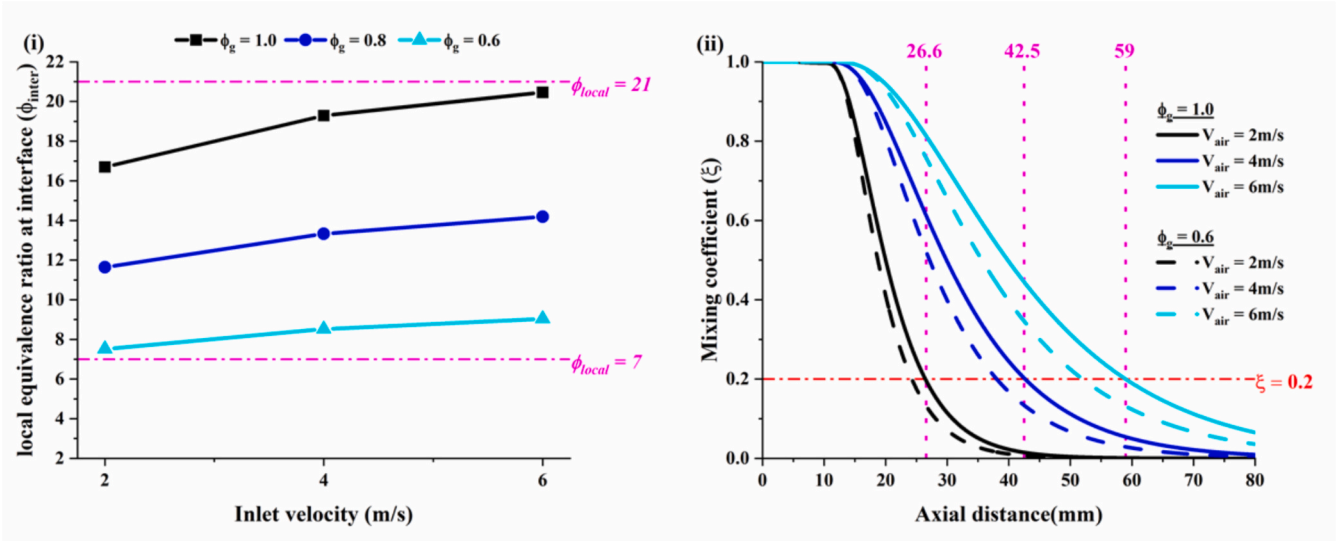

Fig. 5. (i) local equivalence ratio at interface (φ_{inter}) at V_{air} = 2 m/s, 4 m/s and 6 m/s for φ_g = 1.0, 0.8, 0.6 and 0.4 (ii) mixing coefficient (ξ) at V_{air} = 2 m/s, 4 m/s and 6 m/s for φ_g = 1.0 and 0.4.

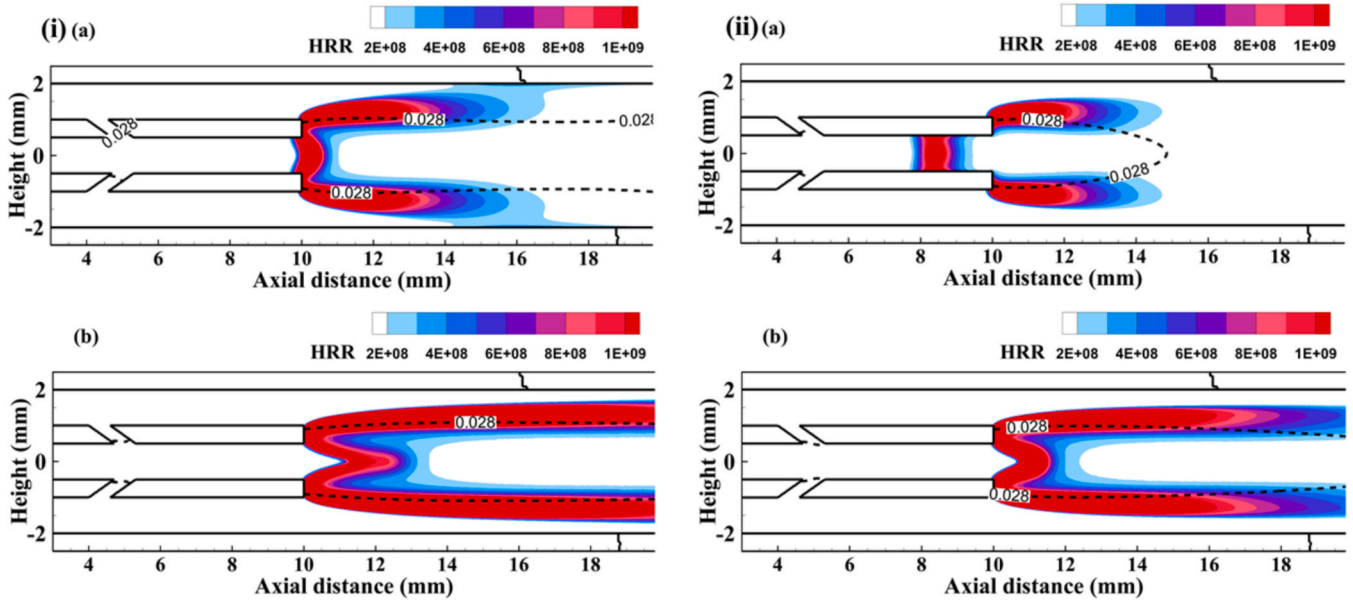

Fig. 6. Variation in flame structure with inlet velocity (a) V_{air} = 2 m/s and (b) V_{air} = 6 m/s at (i) φ_g = 1.0 and (ii) φ_g = 0.6.

partially premixed flame structure attached to the bluff body tip was observed even as the velocity was increased from 2 m/s to 6 m/s. Even though the flame has been stretched downstream at higher velocities, it was well anchored to the bluff body tip. Partially premixed flame is the combination of a radially centered premixed flame and two diffusion flame wings.

$$\text{Mixture fraction, } Z = \frac{\text{mass of material having its origin in the fuel stream}}{\text{mass of mixture}}$$

$$= \frac{MW_{H2}(X_{H2} + X_{H2O} + 0.5\,X_{OH} + 0.5\,X_{HO2} + X_{H2O2})}{MW_{mix}} \quad (8)$$

The value of stoichiometric mixture fraction was calculated to be 0.028 for hydrogen. As shown in the Fig. 5, stoichiometric mixture fraction line denotes the location of diffusion flame front. As the velocity increases, the inner premixed cone and the diffusion wings are significantly stretched.

To further analyze the effect of inlet velocity at lean global equivalence ratios (φ_g = 0.6) on flame structure, HRR at different velocities (2 m/s and 6 m/s) are displayed in Fig. 5 (ii). Interestingly at an inlet velocity of 2 m/s, a diffusion flame with two wings that is attached to the bluff body tip was observed, as demonstrated in Fig. 6 (ii) (a). Additionally, a premixed flame was observed near the bluff body tip in the fuel stream, as a result of partial premixing of air and fuel, which is attributed to the high laminar burning velocity of hydrogen. Furthermore, as the velocity was increased to 6 m/s, the premixed reaction zone reached the bluff body tip and the flame was transformed to a stretched partially premixed flame. This phenomenon ensured that the flame stability will be obviously improved, as the partially premixed flame structure was formed at 6 m/s. The flame length at 6 m/s, φ_g = 0.6 was significantly small (Fig. 6 (ii) (b)) compared to that of φ_g = 1.0 at same velocity (Fig. 6 (i) (b)), which asserts the possibility of high stability limits at low equivalence ratios. The formation of the reaction zone at the micro-mixing slot exit can be explained by the temperature distribution shown in Fig. 8 (i)(b). It is evident that the bluff body tip was heated more than 1200 K. As the rich mixture, resulting from partial premixing, reaches this high-temperature zone, it ignites immediately, leading to the formation of the premixed flame. But due to the very low amount of fuel at low equivalence ratios at low velocity, the reaction occurred was weaker. The increase in velocity to 6 m/s, caused the formation of the large reaction zone, which was reported as the stretched flame. However, the flame is anchored to the bluff body tip at higher velocity due to the partial premixing which is attributed to the unique combustor design.

Fig. 7 (i) and (ii) exhibits the trend in wall temperature distribution along the combustor wall with respect to the variation in inlet velocity and equivalence ratio. When the inlet velocity was increased from 2 m/s to 6 m/s while maintaining a stoichiometric equivalence ratio, the maximum wall temperature increased monotonically and the uniformity in wall temperature improved, which is also reported in the experimental investigation of a micro-combustor by Li et al [56]. At the stoichiometric equivalence ratio, the maximum wall temperature ranged from 1300 K to 1400 K. However, at an equivalence ratio of 0.6, this temperature decreased to 1000 K to 1100 K, as shown in Fig. 7 (i). Nevertheless, the uniformity in wall temperature has significantly improved at lean equivalence ratios, which is a necessary attribute in view of practical applications such as TEG etc. However, when the equivalence ratio was varied keeping velocity constant at 2 m/s and 6 m/s respectively, the maximum wall temperature remained almost same, but the wall temperature uniformity was improved as the velocity increased as shown in Fig. 7 (ii). Most importantly, the uniformity in wall temperature displayed significant improvement at higher inlet velocities (6 m/s).

The variation in temperature contour on the combustor with respect to equivalence ratio are presented in Fig. 8 (i) and (ii). At lower velocities (2 m/s) as the flame was more attached to the bluff body (as seen in Fig. 6 (ii) (a)) and consequently significant hike in bluff body temperature (>800 K) was observed, which is sufficient to initiate the combustion reaction in the fuel stream near the bluff body tip itself. Additionally, as the mixture became leaner (φ_g = 0.6), the premixed flame front moved upstream, which is evident from the temperature distribution on bluff body (Fig. 8 (i) (b) and (ii) (b). The upstream displacement of the diffusion flame was realized by the displacement in stoichiometric mixture fraction line. Even though at higher velocities like 6 m/s, flame stretched downstream, it didn't lift off the bluff body tip as there was sufficient heat transfer from flame to bluff body as displayed in Fig. 8 (i) (a) and (b). Furthermore, at 6 m/s and φ_g = 0.6 (Fig. 8 (ii) (b)) the diffusion flame moved upstream as indicated by the stoichiometric mixture fraction line.

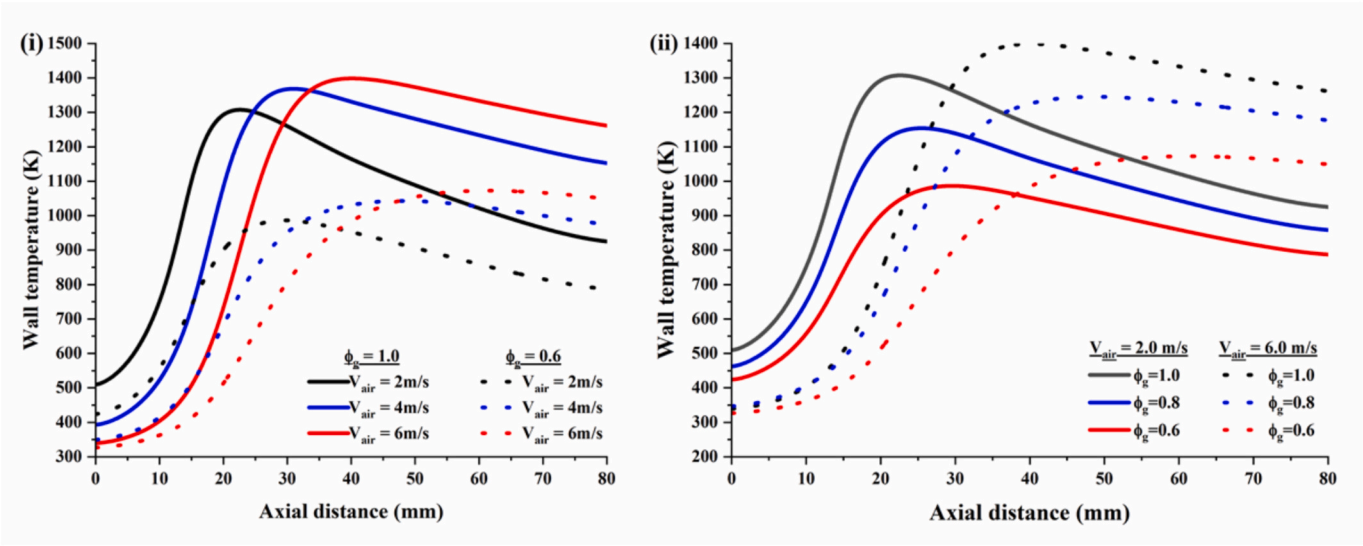

Fig. 7. Wall temperature distribution at (i) V_{air} = 2 m/s, 4 m/s and 6 m/s (maintaining φ_g = 1.0 and 0.4) (ii) φ_g = 1.0, 0.8, 0.6 and 0.4 (maintaining V_{air} = 2 m/s and V_{air} = 6 m/s).

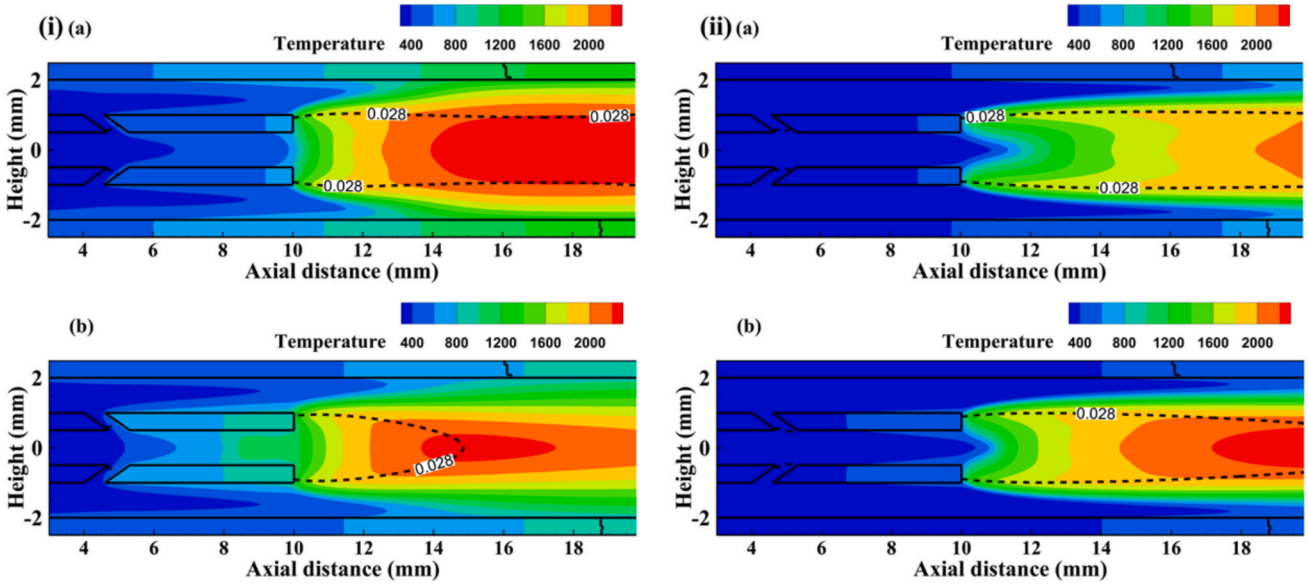

Fig. 8. Variation in temperature distribution with different equivalence ratios (a) φ_g = 1.0 and (b) φ_g = 0.6 at (i) V_{air} = 2 m/s and (ii) V_{air} = 6 m/s.

2.2. *Turbulent flame stabilization characteristics*

Turbulent model was adopted for $V_{air} \geq 8$ m/s due to the higher magnitude Reynold's number (Re > 500). To understand the variation in flame stabilization with inlet velocity and to develop a criterion with non-reacting flow, local equivalence ratio at the central slot interface was tabulated for stoichiometric and lean global equivalence ratios. Inlet velocity was increased at the increment of 2 m/s starting from 8 m/s and cold flow simulations were performed.

2.2.1. *Turbulent local mixing performance*

To establish a correlation between non-reacting and reacting flows for flame stabilization, the local equivalence ratio (φ_{inter}) was calculated for each combination of equivalence ratio and inlet velocity and the results are plotted in Fig. 9. At an inlet velocity of 10 m/s, the cold flow simulation didn't converge and the value of φ_{inter} became very large, indicating that flame had blown off the combustor. However, for lean mixtures (φ_g = 0.8 and 0.6), at elevated velocities up to 14 m/s, cold flow simulations converged and the value of φ_{inter} was observed to be within the specified range. Furthermore, for φ_g = 0.6, the simulations converged up to an inlet velocity of 16 m/s. Interestingly, this criterion aligned with that developed for laminar regime in earlier sections in this article. However, the upper limit (φ_{inter} = 21) shall be refined after determining the exact blow off limit of the combustor at φ_g = 1.0. Further analysis is needed to be conducted to determine the stability limits in terms of equivalence ratio and inlet velocity, which can lead to the refinement of the criterion.

2.2.2. *Effect of inlet velocity on flame stabilization*

The effect of inlet velocity was investigated by presenting the flame structure and temperature profile at inlet velocities 8 m/s and 16 m/s and lean equivalence ratio, φ_g = 0.6. As shown in the Fig. 10 (i) (a) and (b), the flame structure exhibits significant differences in terms of flame length, the way it is attached to the bluff body etc. At an inlet velocity of 8 m/s, the flame is fully attached to the bluff body tip. However, at an elevated velocity of 16 m/s, flame is partially attached to the bluff body

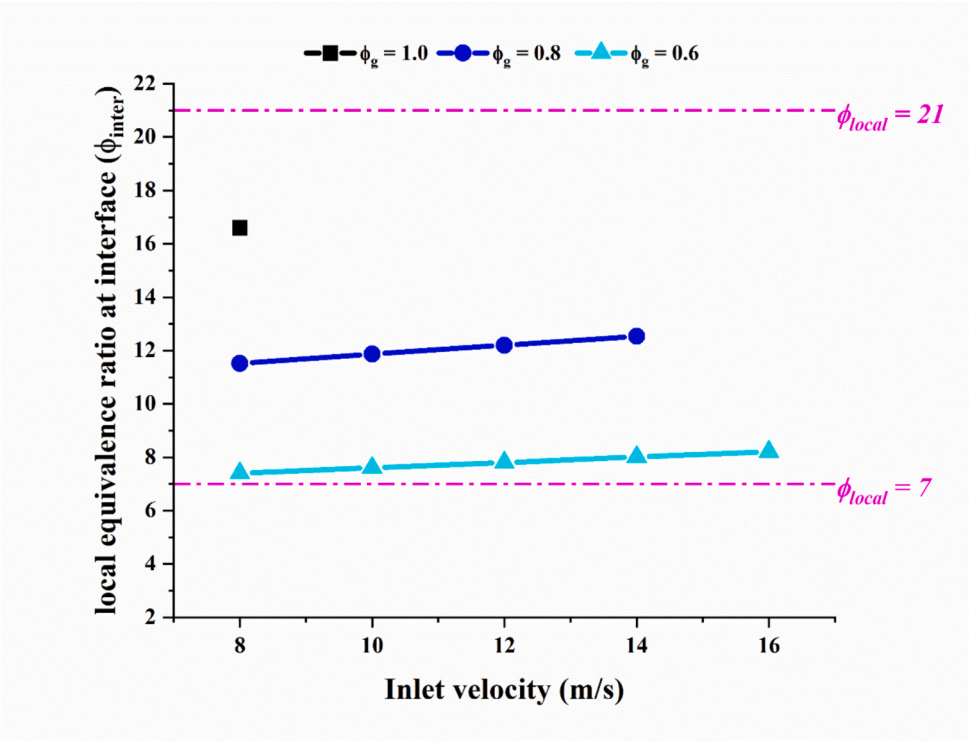

Fig. 9. turbulent local mixing performance at inlet velocities ranging from 8 m/s to 16 m/s.

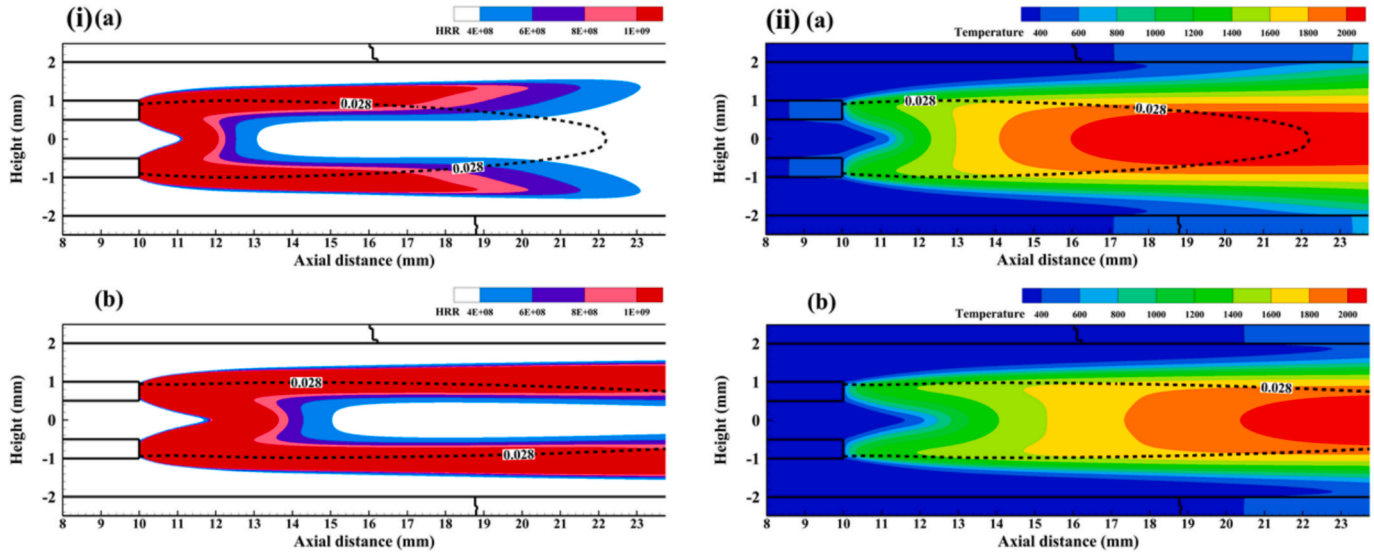

Fig. 10. (i) Flame structure variation and (ii) Temperature distribution with inlet velocity (a) 8 m/s and (b) 16 m/s keeping $\varphi_g = 0.6$.

tip, which indicates that flame is at the verge of lift-off. Additionally, the flame got stretched by the increase of velocity as the flame exhibited significant increase in length. The inner cone of the premixed flame was extended by about 1 mm. Fig. 10 (ii) (a) and (b) show the variation in temperature distribution with inlet velocity. While the bluff body tip was heated to about 600 K due to the heat transfer from flame to bluff body, no such heat transfer was observed at 16 m/s, which suggests the possibility of lift-off with further increase in velocity. Furthermore, the distinction in Z_{stoic} line denoted that although the diffusion flame wings remained at same location, they were stretched significantly.

Flame index is a parameter used to recognize whether a flame is premixed or non-premixed spatially [57]. The expression for flame index (FI) is given as

$$\text{Flame index, FI} = \frac{\nabla Y_F . \nabla Y_O}{|\nabla Y_F||\nabla Y_O|} \tag{9}$$

When the magnitude of flame index is positive, the flame observed is locally premixed, whereas when it is negative, the flame is non-premixed. For instance, FI is plotted to analyze the flame structure in Fig. 11 for the condition $V_{air} = 8$ m/s and $\varphi_g = 0.6$, which indicates that the flame is a combination of central premixed flame cone and two near wall diffusion flame wings.

Fig. 12 demonstrates the trend in wall temperature distribution as the velocity was increased from 8 m/s to 16 m/s ($\varphi_g = 0.6$). The highest wall temperature was observed at the highest velocity of 16 m/s, similar

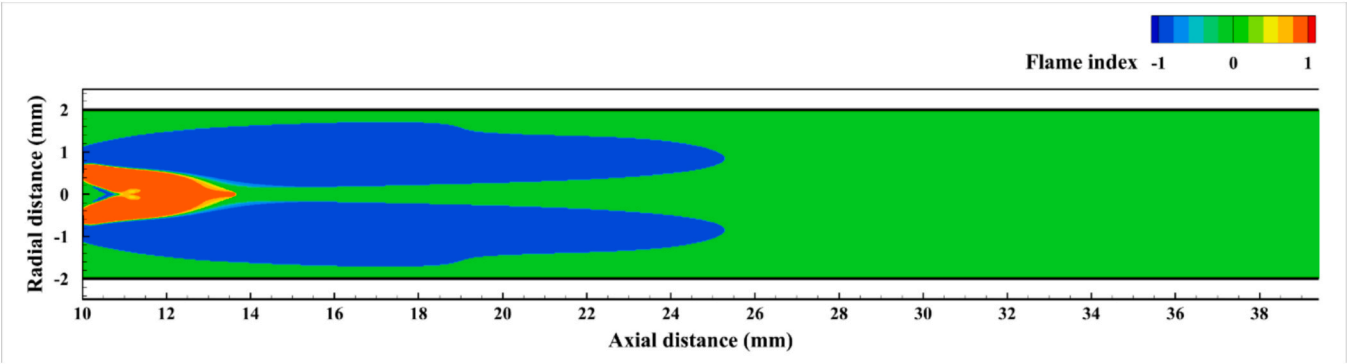

Fig. 11. Flame index at V_{air} = 8 m/s and φ_g = 0.6.

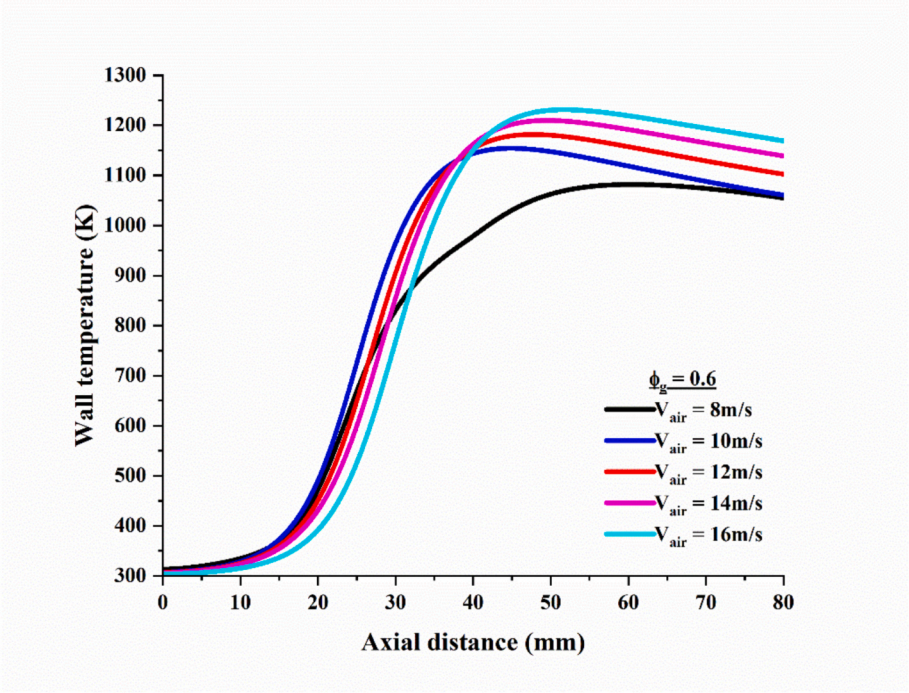

Fig. 12. Variation in wall temperature distribution with inlet velocity keeping φ_g = 0.6.

to the research by Zuo et al [58], but as far as uniformity was concerned, 8 m/s velocity performed significantly better compared to others with a competing maximum temperature of 1000 K, which is sufficient for practical applications like power generation using TEG module. Therefore, for φ_g = 0.6, inlet velocity of 8 m/s shall be considered as the best performer among all velocities, as the authors are keen to develop a micro-power generator with the present micro-combustor by attaching TEG module on the outer walls of the combustor.

2.2.3. *Effect of turbulence on flame stabilization*

The effect of turbulence on flame stabilization was analyzed by examining the behavior of turbulent kinetic energy and velocity vectors on HRR for two cases with the same velocity (V_{air} = 12 m/s) at different lean equivalence ratios (φ_g = 0.8 and 0.6) as shown in Fig. 13 (i) (a) and (b). The flame is observed to be at the verge of lift-off at φ_g = 0.8 (Fig. 13 (i) (a)), as indicated by the inner cone length, stretched flame structure and partial attachment to the bluff body tip. The higher magnitude of turbulent kinetic energy (20 m^2s^{-2}) at an axial location of 18 mm (comparing both cases) ensured better mixing of air and fuel in the former case and the reaction is significantly influenced by turbulence. However, in the latter case (φ_g = 0.6), the reaction is more driven by the mixture leanness as rendered by the flame structure as shown in Fig. 13 (i) (b). The velocity vectors exhibit the same nature in both cases nevertheless. Moreover, the highest magnitude of turbulent kinetic energy in the flame was observed to be 70 m^2s^{-2} at φ_g = 0.8, while the same for φ_g = 0.6 was found to be 30 m^2s^{-2}.

Fig. 13 (ii) (a) and (b) demonstrate the effect of turbulence on temperature distribution, The temperature profile obviously denotes that the flame front moved upstream as the mixture became leaner. The higher magnitude of turbulent kinetic energy lines at the high temperature zone in the former case signifies the relevance of turbulence. However, the velocity vectors in both cases do not exhibit any significant difference. Additionally, at higher temperatures, velocity vectors are having higher magnitudes due to the movement of radicals. To have a further insight into flame stabilization, the comparison of flames with and without micro-mixing is explained in the next section.

2.3. *Effect of micro-mixing on flame formation and stability limits*

In order to understand deeper on flame stabilization through the introduction of micro-mixing, a combustor with identical dimensions without micro-mixing was modeled. Numerical simulations were then

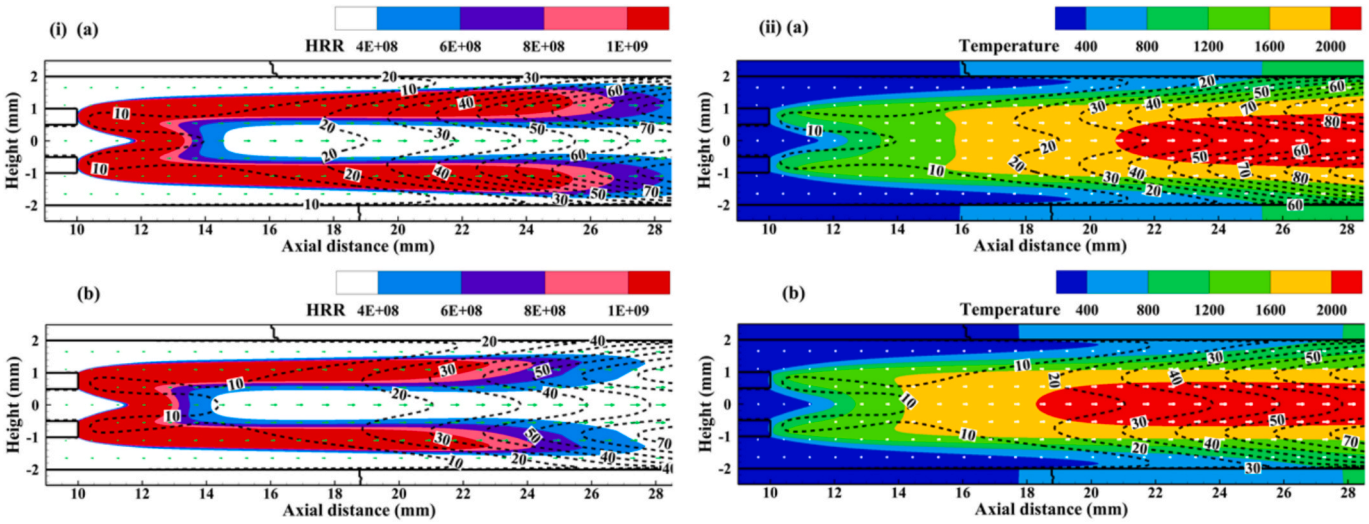

Fig. 13. Effect of turbulent kinetic energy (dashed lines) and velocity vectors (vectors) on (i) flame structure and (ii) temperature distribution at V_{air} = 12 m/s (a) φ_g = 0.8 and (b) φ_g = 0.6.

performed for the same velocity and equivalence ratio (V_{air} = 6 m/s, φ_g = 0.6). Then the flame structure and temperature profile were compared as depicted in Fig. 14 (i) and (ii) respectively. The primary difference observed between Fig. 14 (i) (a) and (b) was the flame structure, as for the former case there was only a diffusion flame while for the latter case there was a partially premixed flame (combination of premixed cone shaped flame and two diffusion flame wings) due to micro-mixing [59]. The secondary fact observed was flame anchoring. In the former case, the flame was partially anchored to the bluff body tip which is a tendency for lift-off. In the latter case flame was anchored completely to the bluff body tip due to relatively low local equivalence ratio at the interface. Furthermore, though the bluff body tip was heated to about 600 K in both cases, for the latter case the heating was extended about 1.75 mm upstream from the bluff body tip. In the former case it was heated for a length of about 3.5 mm, which subsequently enhanced flame stabilization. To have a deeper understanding of this phenomenon, the concentration of species, distribution of mixture fraction and temperature were plotted for the two cases (radial sections A-A and B-B as marked in Fig. 14 (ii) (a) and (b) respectively), in Fig. 15 (i) and (ii).

The trend in distribution of mixture fraction (Z), mole fraction of species (X_{OH}, X_{H2} and X_{o2}) and temperature across radial sections A-A and B-B demonstrate significant difference each other. The magnitude of mixture fraction (Z) became lower (0.1) for the combustor with micro-mixing compared to that of the other combustor (Z = 0.5) due to the partial premixing of air and fuel. X_{H2} also showed a similar reduction from 0.9 to 0.65 by the introduction of micro-mixing. The profile of X_{o2} exhibited an increase at the center due to the micro-mixing. Additionally, the maximum temperature magnitude of diffusion wings remained same but the profile looked different due to the presence of premixed flame.

Finally, the stability limit of the present combustor was compared with the existing ones. But as the combustors vary in height and width, they can't be compared in terms of inlet velocity (blow-off limit). So, the firing rate (in watts) of each combustor at the blow-off condition was calculated. For the sake of comparison, the combustor width is assumed equal (40 mm).

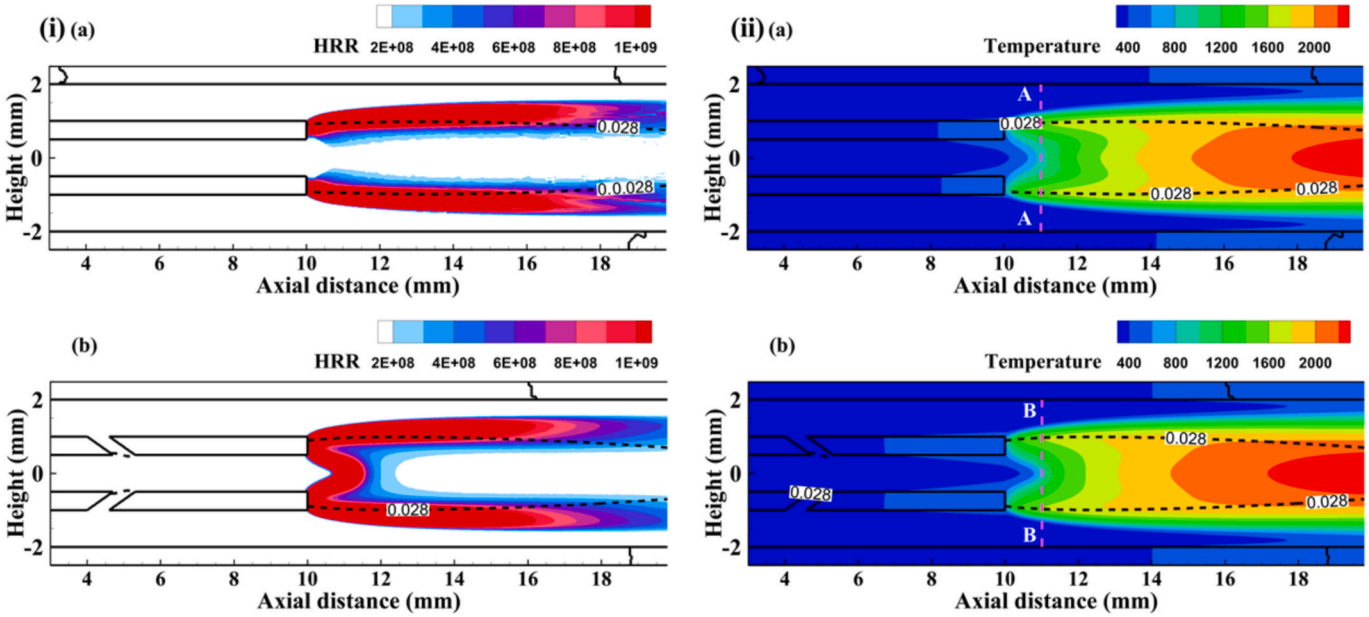

Fig. 14. (i) Flame structure and (ii) Temperature profile at V_{air} = 6 m/s, φ_g = 0.6 (a) without micro-mixing and (b) with micro-mixing.

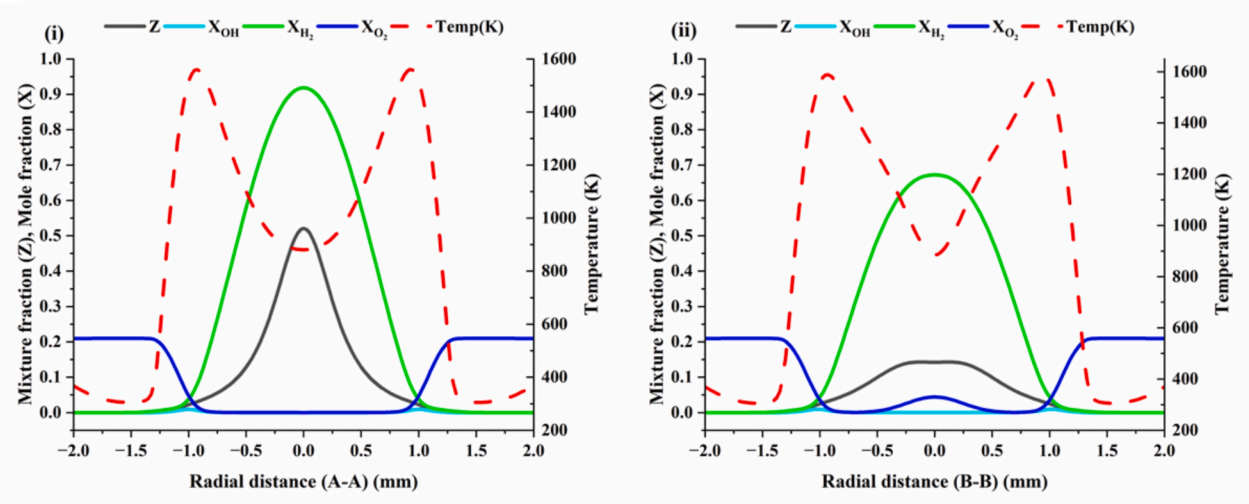

Fig. 15. Comparison of mixture fraction (Z), mole fraction (X) and temperature (i) radially across A-A (NPF) (ii) radially across B-B (PPF).

$$Firing\ rate = Cross\ sectional\ area\ x\ Blow\ off\ velocity\ x\ X_{fuel} x\ CV_{fuel} \quad (9)$$

Wan et al [39] and Fan et al [60] investigated the effect of a triangular bluff body in rectangular combustors (Combustor height, H = 1 mm) and estimated the blow-off limits (52 and 36 m/s) for equivalence ratios (ϕ_g) 0.6 and 0.5 respectively, from which the firing rates were calculated to be 4.52 and 2.70 W. Fan et al [61] also introduced a semicircular bluff body (H = 1 mm) and determined the blow-off limit at $\phi_g = 0.5$ as 43 m/s. The firing rate of the same was computed to be 3.22 W. Lee et al [62] presented the blow off limit (20.6 m/s) by utilizing a square bluff body (H = 1 mm) keeping $\phi_g = 0.5$ and the firing rate was calculated to be 1.54 W. Li et al [28] studied the effect of a slotted bluff body (H = 1.1 mm) on flame stabilization and revealed the blow-off limit at $\phi_g = 0.6$, from which the firing rate was calculated to be 3.25 W. Eventually, as the exact blow-off limit was not determined for the present micro-combustors, the firing rates at lift-off condition (H = 4 mm) were estimated ($\phi_g = 0.6$) as 2.43 and 6.26 W for the combustors without and with micro-mixing respectively. The comparison study revealed that even the lift-off firing rate of the present micro-mixing micro-combustor exhibits a significant hike of 28 % compared to the existing best combustor's blow-off firing rate. Obviously, the difference will be much higher when the exact blow-off limit is determined. Moreover, as discussed in previous sections, the stability limit of the present micro-mixing micro-combustor significantly improves as the mixture gets leaner which indicates that higher blow-off firing rates are possible at lower equivalence ratios.

4. Conclusion

The flame stabilization characteristics of a novel micro-mixing micro-combustor were analyzed. The parameters such as mixing performance, flame structure, flame stabilization, temperature distribution and wall temperature distribution were investigated for both laminar and turbulent flow regimes.

1. The local equivalence ratio at central slot interface (ϕ_{inter}) (cold flow) was observed to be a key factor in flame stabilization of the present micro-combustor. The stable flame region was determined to be within the range $7 < \phi_{inter} < 21$, which holds true for both laminar and turbulent regimes. This criterion is highly relevant, as it allows for the prediction of flame stability limits under cold flow conditions itself.
2. For lean global equivalence ratios ($\varphi_g = 0.6$) at a velocity of 2 m/s, the premixed flame was observed inside the bluff body (fuel stream) and the diffusion flame was anchored to the bluff body tip. When the velocity was increased to 6 m/s the flame was transformed to a partially premixed one which is a combination of premixed cone flame and diffusion flame wings. The wall temperature uniformity exhibited significant improvement as the mixture became leaner, however the magnitude of maximum wall temperature diminished by about 400 K for lean mixtures. For lean mixtures, due to the elevated heat transfer from flame to bluff body, the bluff body temperature increased significantly which subsequently enhanced flame stabilization.
3. Due to the increase in critical Reynold's number, turbulence model was adopted for velocities greater than 6 m/s. Stable flames were achieved for equivalence ratios 1.0 and 0.8 up to 8 m/s and 14 m/s respectively although the exact blow off limits were not determined, which is beyond the scope of the present study. However, $\varphi_g = 0.6$ was stabilized until 16 m/s with a slight indication of lift-off. The study revealed that the present combustor design exhibits excellent flame stabilization characteristics for lean mixtures. The flame structure was more synchronized with turbulent kinetic energy lines as the mixture became richer. The highest magnitude of turbulent kinetic energy in the flame was observed to be 70 m^2s^{-2} at $\varphi_g = 0.8$, while the same for $\varphi_g = 0.6$ was found to be 30 m^2s^{-2}.
4. The effect of micro-mixing on flame formation and the distinction between diffusion and partially premixed flames were compared at combustors with and without micro-mixing at an axial location right downstream the bluff body tip and mixture fraction (Z) and mole fraction of H_2 (X_{H2}) exhibited significant decline of 0.4 and 0.25 due to micro-mixing. Furthermore, even though the magnitude of temperature remained same, temperature profile appeared different due to the difference in flame structure.
5. The stability limit enhancement was analyzed by comparing the blow-off firing rates of the existing combustors with that of the present combustor. The results indicated a significant increase of 28 %, even when the lift-off firing rate of the present micro-combustor was considered. Obviously, the difference will be much higher when the exact blow-off limits are determined.

CRediT authorship contribution statement

Sreejith Sudarsanan: Writing – review & editing, Writing – original draft, Validation, Software, Investigation, Formal analysis, Data curation. **Akram Mohammad:** Writing – review & editing, Supervision, Investigation, Funding acquisition. **Prabhu Selvaraj:** Writing – review & editing, Software, Resources, Investigation, Conceptualization. **Khalid A. Juhany:** Writing – review & editing, Project administration,

Investigation, Funding acquisition. **Radi A. Alsulami:** Writing – review & editing, Funding acquisition, Formal analysis, Conceptualization. **Sudarshan Kumar:** Writing – review & editing, Supervision, Project administration, Conceptualization. **Ratna Kishore Velamati:** Writing – review & editing, Supervision, Project administration, Investigation, Funding acquisition, Data curation, Conceptualization.

Declaration of competing interest

The authors declare that they have no known competing financial interests or personal relationships that could have appeared to influence the work reported in this paper.

Acknowledgements

The authors gratefully acknowledge the support partial funding from the Science and Engineering Research Board (SERB), Department of Science & Technology (DST), Govt of India, under grant number CRG/2021/003079, through the Core research grant scheme.

This research work was also funded by Institutional Fund Projects under grant no. (IFPRC-111-135-2020). Therefore, authors gratefully acknowledge technical and financial support from the Ministry of Education and King Abdulaziz University, Jeddah, Saudi Arabia.

Data availability

Data will be made available on request.

References

[1] Guo L, et al. Methane-air partially premixed flame behaviors in a micro plate slit. Chem Eng Process - Process Intesif 2020;158.
[2] Zha H, Zhao D, Becker S. Thermal performances investigation on an ammonia-fuelled heat-recirculating micro-combustor with reduced chemical mechanism. Appl Therm Eng 2024;236.
[3] Cai T, Zhao D. Enhancing and assessing ammonia-air combustion performance by blending with dimethyl ether. Renew Sustain Energy Rev 2022;156:112003.
[4] Cai T, et al. Removal and mechanism analysis of NOx emissions in carbon-free ammonia combustion systems with a secondary fuel injection. Fuel 2023;344:128088.
[5] Cai T, Zhao D, Gutmark E. Overview of fundamental kinetic mechanisms and emission mitigation in ammonia combustion. Chem Eng J 2023;458:141391.
[6] Balaji RK, Rajan KP, Ragula UBR. Modeling & optimization of renewable hydrogen production from biomass via anaerobic digestion & dry reformation. Int J Hydrogen Energy 2020;45(36):18226–40.
[7] Sudarsanan S, et al. Impact of H2 blending of methane on micro-diffusion combustion in a planar micro-combustor with splitter. Energies 2024;17(4).
[8] Sankar V, Mukhopadhyay S, Velamati RK. Enhancement of radiative power using a divergent splitter plate design in H2-air non-premixed micro-combustor. J Energy Res Technol 2024;146(4).
[9] Radhika N, et al. High entropy alloys for hydrogen storage applications: A machine learning-based approach. Results Eng 2024;23.
[10] Raghavan KAS, Rao SS, Raju VRK. Effect of deflector on the combustion characteristics of a micro-combustor with a controlled centrally slotted bluff body. J Energy Resour Technol Trans ASME 2024;146(2).
[11] Cai S, Yang W, Wan J. Combustion and thermal performances of methane-air premixed flame in a novel preheated micro combustor with a flame holder. Int J Therm Sci 2024;197.
[12] Booma Devi P, et al. Positional effect of vortex generators on the combustion efficiency of the micro combustor fuelled with hydrogen/air mixture. Fuel 2024;358.
[13] George LK, et al. Unsteady dynamics in a subsonic duct flow with a bluff body. Phys Fluids 2022;34(6).
[14] Luckachan KG, et al. Transient vortex shedding behaviour of non-reacting flow over V-gutter bluff bodies with a central slit. Int J Ambient Energy 2022;43(1):8686–96.
[15] Sankar V, et al. Towards the development of miniature scale liquid fuel combustors for power generation application—a review. Energies 2023;16(10).
[16] Tang A, et al. A comparative study on combustion characteristics of methane, propane and hydrogen fuels in a micro-combustor. Int J Hydrogen Energy 2015;40(46):16587–96.
[17] Srinivasa Raghavan KA, Srinivasa Rao S, Raju VRK. Numerical investigation of the effect of the slit profile on the combustion characteristics of a micro-combustor with a centrally slotted bluff body. Proc Inst Mech Eng Part E J Process Mech Eng 2023;237(3):917–27.
[18] Zuo W, et al. Numerical investigations on hydrogen-fueled micro-cylindrical combustors with cavity for micro-thermophotovoltaic applications. Energy 2021;223.
[19] Lu Q, et al. Numerical study on hydrogen heterogeneous reaction characteristic in a micro catalytic combustor with blunt body. Fuel 2024;357.
[20] Ding J, et al. Effect analysis on energy conversion enhancement of porous medium micro-combustor and thermoelectric system and its optimization. Energ Conver Manage 2023;292.
[21] Ni S, Zhao D. NOx emission reduction in ammonia-powered micro-combustors by partially inserting porous medium under fuel-rich condition. Chem Eng J 2022;434:134680.
[22] Lachraf A, Si Ameur M. Numerical investigation of thermal performance of hydrogen fueled micro-combustor with trapezoidal ribs. Int J Hydrogen Energy 2023;48(99):39570–85.
[23] Luo B, et al. Effects of different channels on performance enhancement of a nozzle hydrogen-fueled micro combustor for micro-thermophotovoltaic applications. Int J Hydrogen Energy 2023;48(54):20743–61.
[24] Zhao H, et al. NO emission and enhanced thermal performances studies on Counter-flow Double-channel Hydrogen/Ammonia-fuelled microcombustors with Oval-shaped internal threads. Fuel 2023;341.
[25] Wang S, Li J, Fan A. Effects of channel height on the combustion efficiency and thermal performances of a micro Swiss-roll combustor. Appl Therm Eng 2024;238.
[26] He Z, et al. Numerical investigation of a novel micro combustor with a central and bilateral slotted blunt body. Int J Hydrogen Energy 2021;46(45):23564–79.
[27] Raghavan KAS, Rao SS, Raju VRK. Numerical investigation of the effect of slit-width on the combustion characteristics of a micro-combustor with a centrally slotted bluff body. Int J Hydrogen Energy 2023;48(14):5696–707.
[28] Li L, Fan A. A numerical study on non-premixed H2/air flame stability in a micro-combustor with a slotted bluff-body. Int J Hydrogen Energy 2021;46(2):2658–66.
[29] Basak AK, et al. Bound metal deposition of stainless steel 316L: Effect of process variables on microstructural and mechanical behaviors. Materialia 2024;36.
[30] Yuliati L, Sasongko MN, Wahyudi S. Flammability limit and flame visualization of gaseous fuel combustion inside meso-scale combustor with different thermal conductivity. Applied mechanics and materials. 2014.
[31] Liu L, Zhao L, Fan AW. Effects of wall thickness and material on flame stability in a planar micro-combustor. J Cent South Univ 2019;26(8):2224–33.
[32] Tian X, et al. Improvement of energy conversion of H2/CH4 fueled micro-thermophotovoltaic in a micro-planar inserted with bluff-body and porous media. Appl Therm Eng 2024;236.
[33] Mokrin SN, et al. Flammability limit of moderate- and low-stretched premixed flames stabilized in planar channel. Combust Flame 2017;185:261–4.
[34] Wan J, Zhao H. Laminar non-premixed flame patterns in compact micro disc-combustor with annular step and radial preheated channel. Combust Flame 2021;227:465–80.
[35] Kang X, et al. A numerical investigation on the thermo-chemical structures of methane-oxygen diffusion flame-streets in a microchannel. Combust Flame 2019;206:266–81.
[36] Yang H, et al. Partially-Premixed Combustion Characteristics and Thermal Performance of Micro Jet Array Burners with Different Nozzle Spacings. J Therm Sci 2021;30(5):1718–30.
[37] Chen X, et al. Effects of porous media on partially premixed combustion and heat transfer in meso-scale burners fuelled with ethanol. Energy 2021;224.
[38] Ghai SK, De S. Numerical investigation of flow and scalar fields of piloted, partially-premixed dimethyl ether/air jet flames using stochastic multiple mapping conditioning approach. Combust Flame 2019;208:480–91.
[39] Wan J, et al. Experimental and numerical investigation on combustion characteristics of premixed hydrogen/air flame in a micro-combustor with a bluff body. Int J Hydrogen Energy 2012;37(24):19190–7.
[40] Wan J, et al. Hydrogen-enriched flames in a novel miniature double-layer disc-combustor with annular step and Swiss-roll preheated channel. Combust Flame 2023;251.
[41] Ma L, et al. Influence of CH4/air injection location on non-premixed flame blow-off limits in a novel micro-combustor. Int J Hydrogen Energy 2022;47(9):6323–33.
[42] Xing C, et al. Effect of fuel flexibility on combustion performance of a micro-mixing gas turbine combustor at different fuel temperatures. J Energy Inst 2022;102:100–17.
[43] Hussain M, et al. Micromixers and hydrogen enrichment: The future combustion technology in zero-emission power plants. American Society of Mechanical Engineers, Power Division (Publication) Power. 2020.
[44] Liu X, et al. Cold flow characteristics of a novel high-hydrogen Micromix model burner based on multiple confluent turbulent round jets. Int J Hydrogen Energy 2021;46(7):5776–89.
[45] Kuo CH, Ronney PD. Numerical modeling of non-adiabatic heat-recirculating combustors. Proc Combust Inst 2007;31(II(2)):3277–84.
[46] Quaye EK, et al. Geometrical optimization of premixed hydrogen-air combustion in a novel counter-flow preheating micro-combustor. Energy 2024;313:133897.
[47] Yan Y, et al. Numerical study on methane/air combustion characteristics in a heat-recirculating micro combustor embedded with porous media. Int J Hydrogen Energy 2022;47(48):20999–1012.
[48] Wang S, Yuan Z, Fan A. A modified two-dimensional numerical method for prediction of outer wall temperature distribution of rectangular micro-combustors. Int J Hydrogen Energy 2019;44(31):16983–90.
[49] Ansys. *Species transport and multi component diffusion equations*. 2009.
[50] Kéromnès A, et al. An experimental and detailed chemical kinetic modeling study of hydrogen and syngas mixture oxidation at elevated pressures. Combust Flame 2013;160(6):995–1011.

[51] Liu YF, et al. Experimental investigation of emissivity of steel. Int J Thermophys 2013;34(3):496–506.
[52] Liu H, Zeng Z, Guo K. Numerical investigation of the hydrogen swirl combustion flow in a micro gas turbine burner. Proc Inst Mech Eng, Part A: J Power Energy 2022;236(8):1633–49.
[53] Liu H, Zeng Z, Guo K. Numerical analysis on hydrogen swirl combustion and flow characteristics of a micro gas turbine combustor with axial air/fuel staged technology. Appl Therm Eng 2023;219.
[54] Meier W, et al. Characterization of turbulent hytVAir jet diffusion flames by single-pulse spontaneous raman scattering. Combust Sci Technol 1996;118(4–6):293–312.
[55] Li L, et al. Numerical investigation on mixing performance and diffusion combustion characteristics of H2 and air in planar micro-combustor. Int J Hydrogen Energy 2018;43(27):12491–8.
[56] Li J, et al. Experimental investigation of porous media combustion in a planar micro-combustor. Fuel 2010;89(3):708–15.
[57] Mandal A, et al. Flame stabilization and formation of flame street in a H2/Air non-premixed micro-combustor with a bluff body. Int J Hydrogen Energy 2024;58:1149–59.
[58] Zuo W, et al. Numerical investigations on different configurations of a four-channel meso-scale planar combustor fueled by hydrogen/air mixture. Energ Conver Manage 2018;160:1–13.
[59] Aggarwal SK. Extinction of laminar partially premixed flames. Prog Energy Combust Sci 2009;35(6):528–70.
[60] Fan A, et al. The effect of the blockage ratio on the blow-off limit of a hydrogen/air flame in a planar micro-combustor with a bluff body. Int J Hydrogen Energy 2013;38(26):11438–45.
[61] Fan A, et al. Effect of bluff body shape on the blow-off limit of hydrogen/air flame in a planar micro-combustor. Appl Therm Eng 2014;62(1):13–9.
[62] Lee BJ, Yoo CS, Im HG. Dynamics of bluff-body-stabilized premixed hydrogen/air flames in a narrow channel. Combust Flame 2015;162(6):2602–9.